GenHel S-76C Model Correlation using Flight Test Identified Models

Chris Quiding
Handling Qualities Engineer
Sikorsky Aircraft Corporation
Stratford, C
cquiding@sikorsky.com

Christina M Ivler
Aerospace Engineer
Aeroflightdynamics Directorate (AMRDEC)
US Army Research, Development, and Engineering Command
Ames Research Center, Moffett Field, CA
civler@mail.arc.nasa.gov

Dr. Mark B. Tischler
Senior Scientist and Flight Control Group Lead
Aeroflightdynamics Directorate
US Army Research, Development, and Engineering Command
Ames Research Center, Moffett Field, CA
mtischler@mail.arc.nasa.gov

Abstract

γ	Lock number
ζ_{llr}	Lag regressive mode damping ratio
ζ_p, ζ_q	Damping ratios of lead-lag dipole numerators
η_{C_T}	Integrated perturbation thrust coefficient
$\eta_{X_{C'}}$	Lagged collective state
θ, ϕ, ψ	Pitch, roll and yaw attitudes (earth-fixed coordinate system)
υ	Rotor inflow
υ_ζ	Lag regressive mode frequency in rotating frame
σ_{llr}	Real part of lag regressive mode eigenvalue
τ_f	Flapping time constant
$\omega_{d_{llr}}$	Imaginary part of lag regressive mode eigenvalue
ω_{llr}	Lag regressive mode natural frequency
ω_p, ω_q	Natural frequencies of lead-lag dipole numerators
Ω	Main rotor speed

Introduction

The Sikorsky S-76® is a light twin-engine helicopter originally designed and certified in the 1970s. Subsequent updates have been undertaken on the S-76 over the last 30 years to increase the capability of the

2. State Space Model Identification

Model parameters are optimized to provide the best match to frequency responses identified from flight data. A coherence weighted cost function (J) is used to quantify the match between flight data and the state-space model. Then the theoretical accuracy parameters, Insensitivity (I) and Cramer Rao Bound (CR), are used to evaluate the uniqueness of each parameter. Insensitivity is measure of the insensitivity of the cost function to a percent change in the identified parameter. A Cramer Rao Bound is the estimated minimum standard deviation of a parameter that would be calculated after many repeated trials.

3. Time Domain Verification

The state-space model is driven with flight data (not used in the identification), and the outputs of the model are evaluated against the real flight data. Doublets in each axis are usually used for verification.

This paper will discuss these steps for both the hover and 120 kts identifications of the S-76C++ helicopter.

Hover Model Identification

The hover model was identified using piloted frequency sweeps of the longitudinal cyclic stick, lateral cyclic stick, collective stick and pedals respectively. Frequency sweep techniques developed over many years of system identification work by the U.S. Army Aeroflightdynamics Directorate (AFDD) were employed in these flight tests. These methods are described in Ref. 1. The S-76C++ test aircraft was fully instrumented during the flight tests and the hover model identification flight test data was sent to AFDD for a hover higher order hybrid model identification. Sikorsky did parallel quasi-steady model identification at hover (6 DOF) for comparison purposes, but the results are not shown herein.

Frequency Response Determination

Frequency responses were identified from flight data using the methods discussed in the previous section of this paper. For the analysis, the input signals were the piloted inputs X_A, X_B, X_C and

Engine Dynamics

As shown in Fig. 4, the r/X_C phase rolls off very quickly at high frequencies. This is well known (see Ref .1) as an effect associated with engine dynamics. These dynamics can be modeled as a time delay on the r/X_C pairing. Thus, a padé approximation was included in the state-space model structure to represent the engine effect on the yaw response.

Coning-Inflow Dynamics

Figure 5 shows the response of vertical acceleration (a_z) to collective input for the hover flight condition. The rising magnitude response above about 2 rad/s is the result of the coning-inflow dynamics. This rise in magnitude cannot be represented within a quasi-steady model structure. Therefore, a representation of coning-inflow dynamics were necessary in the model structure.

Hybrid Model Structure

The hybrid model structure discussed in Ref. 1 was used for this model identification. The term "hybrid" indicates that the low frequency velocity effects are represented by quasi-steady derivatives (e.g. L_v and M_u), while short term dynamics are modeled with explicit rotor states and associated derivates (e.g. $L_{\beta 1s}$). The hybrid S-76 model was identified with flapping dynamics, coning-inflow dynamics, and engine dynamics. The lag-regressive mode dynamics were identified in the model as a filter on the rate outputs. The equations for the model are given in Ref 1.

The model structure used for identification is:

$$M\dot{x} = Fx + Gu \tag{4}$$

$$y = H_0 x + H_1 \dot{x} \tag{5}$$

The state, input and output vectors for this model identification are:

$$\begin{aligned} x = [&u \quad v \quad w \quad p \quad q \quad r \quad \phi \quad \theta \quad \beta_{1s} \quad \beta_{1c} \\ &u_m \quad v_m \quad \upsilon \quad \dot{\beta}_0 \quad \beta_0 \quad \eta_{C_T} \quad x_e \quad \eta_{X_{C'}}] \end{aligned} \tag{6}$$

$$u = \left[X_A \quad X_B \quad X_C \quad X_P\right] \tag{7}$$

$$\begin{aligned} y = [&\dot{u}_m \quad \dot{v}_m \quad \dot{w} \quad p \quad q \quad r \\ &a_{x_m} \quad a_{y_m} \quad a_z \quad \left(a_{y_m}\right)_2] \end{aligned} \tag{8}$$

The measured accelerations were not taken at the vertical center of gravity, therefore an estimate of the vertical c.g. offset of the measurement (Z_{accel}) was identified in the state equations:

$$\dot{u}_m - \dot{u} - \dot{q} Z_{accel} = 0 \tag{9}$$

$$\dot{v}_m - \dot{v} + \dot{p} Z_{accel} = 0 \tag{10}$$

The lead-lag dynamics primarily influence the on-axis responses in pitch rate and roll rate and can be well represented as a complex dipole. This dipole is applied as a filter on the on-axis angular responses to the lateral and longitudinal stick inputs. The transfer functions used to perform this fit are presented below.

$$\left.\frac{q}{X_B}\right|_{lead-lag} = \frac{q}{X_B} * \frac{K_q(s^2 + 2\zeta_q \omega_q s + \omega_q^2}{s^2 + 2\zeta_{ll_r} \omega_{ll_r} s + \omega_{ll_r}^2} \tag{11}$$

$$\left.\frac{p}{X_A}\right|_{lead-lag} = \frac{p}{X_A} * \frac{K_p(s^2 + 2\zeta_p \omega_p s + \omega_p^2}{s^2 + 2\zeta_{ll_r} \omega_{ll_r} s + \omega_{ll_r}^2} \tag{12}$$

Equations (11) and (12) are implemented in canonical form as shown for the pitch case:

$$\begin{aligned} &\begin{bmatrix} 1 & 0 & 0 \\ 0 & 1 & 0 \\ 0 & -1 & 1 \end{bmatrix} * \begin{bmatrix} (\dot{x}_1)_q \\ (\dot{x}_2)_q \\ \dot{\eta}_{q_{ll}} \end{bmatrix} = \\ &\qquad \begin{bmatrix} 0 & 1 & 0 \\ -\omega_{ll_r}^2 & -2\zeta_{ll_r}\omega_{ll_r} & 0 \\ \omega_q^2 & 2\zeta_q \omega_q & 0 \end{bmatrix} * \begin{bmatrix} (x_1)_q \\ (x_2)_q \\ \eta_{q_{ll}} \end{bmatrix} + \begin{bmatrix} 0 \\ K_q \\ 0 \end{bmatrix} [q] \end{aligned} \tag{13}$$

where, $\dot{\eta}_{q_{ll}} = q_{lead-lag}$.

A similar setup is used for the roll case, where the regressive lag damping and natural frequency is

Model Structure Determination

Many of the higher order effects modeled in hover tend to wash out in forward flight. To determine which (if any) higher order dynamics were necessary for the 120kts flight cond

Chapter 5 of Ref. 7. The reference indicates that this nonlinearity is likely due to tail/empennage interaction with the main rotor wake. Despite the presence of these nonlinear dynamics, the goal was to provide the best possible linear representation of the system. When dynamics are nonlinear, the frequency response as obtained from a Fourier transform is the first harmonic component of a Fourier series, and constitutes the describing function that best characterizes the nonlinear behavior (Ref. 8, Ref. 1). So, the state-space model resulting from frequency response identification is the best linear representation of the nonlinear dynamics.

Model Verification

When the time domain verification of the model was initially performed, it was evident that the model did not predict the damping of the Dutch roll mode correctly. The angular rate response to an initial pedal doublet is shown in Fig. 13. It can be seen in this plot that the identified model predicted too much damping of the Dutch roll mode.

Another difficulty in the verification was due to the nonlinearity observed at the Dutch roll frequency in the previous section of this paper. The verification results from the model confirmed that this motion is nonlinear because of the differences between the Dutch roll mode damping and frequency for two doublets (one right, one left) at the same flight condition. Figure 14 shows that the Dutch-roll mode of the model appears to have a frequency that is lower than flight in the first doublet, and in the second doublet the frequency seems to be higher than flight. This discrepancy shows the presence of nonlinearities because different inputs create varying dynamic characteristics in the response. In the first doublet, we see that the flight response seems to be getting smaller (positive damping ratio) for the first cycles, and then in the last cycle the responses seems to be growing (negative damping ratio). A similar characteristic is shown for high speed Puma Helicopter flight data in Ref. 7, caused by interference effects of the main wake on the tail/empennage. This implies that the Dutch roll mode dynamics of the S-76 are also being affected by the main rotor wake.

Following investigation of the Dutch roll mode, it was necessary to correct the identified model such that the damping of the Dutch roll mode was better represented on average. Ref. 7 provided equations that showed the damping of the Dutch roll mode was largely affected by the N_r derivative.

The N_r derivative was reduced in the identified model

be the inclusion of aerodynamic phase lag into the model and the inclusion of a destabilizing yaw damping map.

Off-Axis Responses

GenHel has historically been unable to predict off-axis responses to control inputs. Ref. 10 theorized that the reasons for this in different flight regimes was as follows:

1. Hover and low speed flight

The unmodeled effect of geometric wake distortion caused by rotor flapping is the reason for GenHel not correctly predicting the off-axis responses.

2. High speed flight

The 2-D unsteady aerodynamic response associated with the shed wake is the source of the discrepancy between GenHel and flight test data for off-axis responses.

A method that has been used in Ref. 10 to correct this issue is the use of aerodynamic phase lag. Calculation of the aerodynamic forces for each blade element in GenHel is performed using airfoil maps. For a given blade element at a given time, the aerodynamic forces (lift, drag and moment) acting on the blade element are found by using the local angle of attack and Mach number to find the non-dimensional lift, drag and moment coefficients for the blade segment's respective airfoil.

Aerodynamic phase lag manipulates the aerodynamic force lookups for each blade element to cause an effective phase shift in the aerodynamic forcing function on the rotor. The effective phase shift in the aerodynamic forcing function causes the responses to control inputs to be shifted in phase. For longitudinal stick inputs, this phase shift would be most clearly seen in the roll rate response to longitudinal stick input frequency response pair. This is because the roll inertia of the S-76 is significantly less than the pitch intertia. Thus, small changes in the phasing of the aerodynamic forcing function are most notably seen in this off-axis response.

The first step in implementing aerodynamic phase lag was to compare the GenHel S-76C model to flight test data in the frequency domain. This comparison was performed by applying frequency sweeps of the longitudinal stick to the GenHel S-76C model. The data generated from the frequency sweeps was then compared to the longitudinal stick frequency sweeps from the S-76C++ flight test data.

Figure 20 shows the roll rate response to longitudinal stick frequency response pair comparison between the S-76C++ flight test data (solid line) and the GenHel S-76C model (dashed line) for the hover flight condition. It can be seen in the plot that the phase of the GenHel S-76C model differs significantly from the flight test data for frequencies above 1 rad/s. Also, the magnitude of the GenHel S-76C model is a factor of 4-6 (12-18 dB) less than the test data across all frequencies. This frequency domain comparison were consistent with the GenHel time domain results seen previously in Fig. 18.

Figure 21 below shows the roll rate response to longitudinal stick frequency response pair comparison between the S-76C++ flight test data (solid line) and the GenHel S-76C model (dashed line) for the 120 knot level flight condition. It can be seen in the plot that the phase of the GenHel S-76C model is similar to the test data across all frequencies. However, the magnitude was a factor of 4-8 times less in the GenHel S-76C model when compared to the test data.

To improve the off-axis response in hover, a range of aerodynamic phase lag settings were tested. These phase lags ranged from 10 to 50 degrees in increments of 10 degrees. For each aerodynamic phase lag angle, frequency sweeps of the longitudinal stick were applied to the GenHel S-76C model in hover. The GenHel data for all the angles was then collected and overlaid with the test data. Following this comparison, it was found that 40 degrees of aerodynamic phase lag provided the most improvement in magnitude and phase for the hover flight condition.

A comparison plot of the flight test data (solid line), GenHel S-76C model without aerodynamic phase lag (dashed line) and the GenHel S-76C model with 40 degrees of aerodynamic phase lag (broken dashed line) for the roll rate response to longitudinal stick frequency response pair is shown in Fig. 22. It can be seen that the phase was significantly improved with the use of 40 degrees of aerodynamic phase lag in hover. While the magnitude was improved, it was still 2-4 times less than the flight test data.

The frequency domain comparisons showed that the roll rate response to longitudinal stick was improved in hover for the GenHel S-76C model with the inclusion of 40 degrees of aerodynamic phase lag. It was important to verify these improvements by performing time domain comparisons between the GenHel S-76C model and flight test data. A time history comparison showing the pitch rate and roll rate responses to a longitudinal stick doublet is shown in Fig. 23. It can be seen in the plot that the frequency domain results were confirmed in the time domain. The phase of the off-axis response was significantly improved and a small improvement in magnitude also occurred.

The approach used in hover was also used in an attempt to improve off-axis responses in the GenHel S-76C model at high speed (i.e. 120 knots). Aerodynamic phase lag between 10 and 30 degrees in increments of 10 degrees were put into the GenHel S-76C model. For each increment, frequency sweeps of the longitudinal stick were performed with the GenHel S-76C model.

The data was then collected and compared to the flight test data. Following this co

Speeds above 120 knots were not tested during the S-76C++ flight test program for safety of flight concerns. Therefore, it was necessary to use previous S-76 test data to estimate the damping of the Dutch roll mode at higher flight speeds. This estimate of damping was then to be used as a basis for choosing the yaw damping map for higher airspeeds in the GenHel S-76C model.

Pedal pulse data at 150 knots was collected during an S-76A flight test program conducted in 1977. Unfortunately, this test data was not available in an electronic format. Therefore, a visual assessment of the test data was made and it was estimated that the damping ratio of the S-76 Dutch roll mode at 160 knots was approximately -0.1. Because no time domain comparisons could be performed at higher speeds, the yaw damping map was adjusted until the damping ratio of the Dutch roll mode in the GenHel S-76C model was near -0.1 at higher airspeeds.

Altogether, yaw damping maps were determined at 80 knots, 120 knots and 160 knots. These maps were combined to form the yaw damping map for the GenHel S-76C model. The yaw damping maps determined for the GenHel S-76C model at 80 and 160 knots are presented in Fig. 30.

Since the yaw damping maps were defined for three specific airspeeds, linear interpolation within the GenHel software was used to determine the yaw damping maps for other airspeeds. Because of this interpolation, it was necessary to check that the progression of the Dutch roll mode eigenvalues with airspeed was sensible (i.e. smooth variation with airspeed). To perform this check, linear models were extracted from the GenHel S-76C model for speeds from 80 to 160 knots in increments of 10 knots. The eigenvalues for each condition were then overlaid with one another such that a locus of the Dutch roll mode eigenvalues with airspeed was clear. This plot is presented in Fig. 31. It can be seen in the plot that the progression of the Dutch roll mode eigenvalues was smooth from 80 – 160 knots. Therefore, it could be concluded that the inclusion of the yaw damping map achieved the desired objective of improving the GenHel S-76C model's ability to predict the damping of the Dutch roll mode.

Conclusions/Recommendations

System identification of two flight conditions, hover and 120 knots, were successfully completed using frequency domain system identification methods. The resulting linear models provided physically meaningful models that were used to correct the S-76C GenHel nonlinear math model. A summary of lessons learned from this effort are:

1. CIFER® frequency irspeu(-134.3(n)6(f6(S-7m)1iti(d)3sal51345e]

1.

helicopter", AHS, Annual Forum, 46th, Washington, DC; UNITED STATES; 21-23 May 1990. pp. 99-137. 1990.

[4] Harding, Jeff, Moody, Scott, "Identification of AH-64D Dynamics to Support Flight Control System Evaluations," Proceedings of the American Helicopter Society 61st Annual Forum, Grapevine, Texas, June 1-3 2005.

[5] Christensen, K. T., Campbell, K. G., Griffith, C. D., Ivler, C. M., Tishcler, M. B., Harding, J. W., "Flight Control Development for the ARH-70 Armed Reconnaissance Helicopter Program", American Helicopter Society 63rd Annual Forum, Virginia Beach,

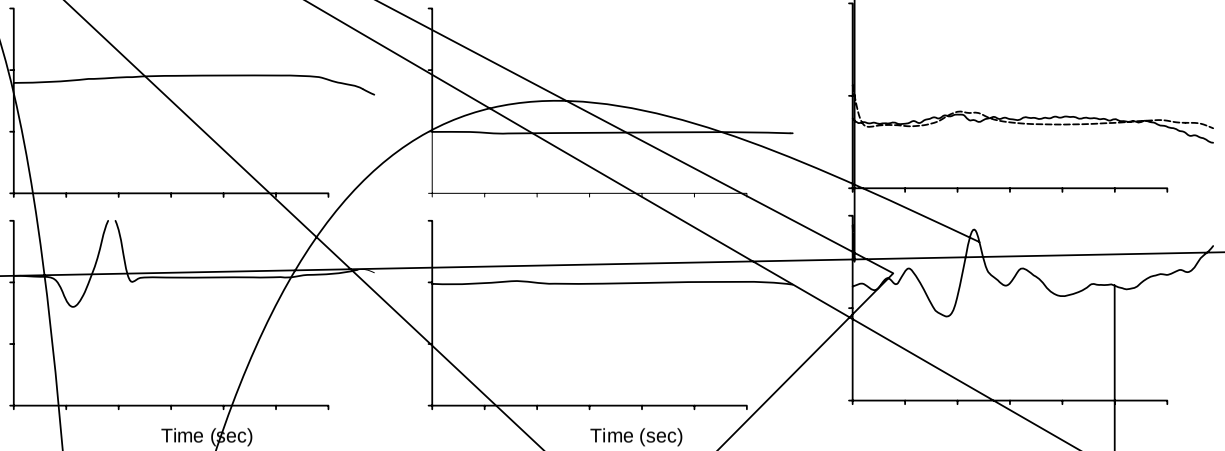
Time (sec)
Time (sec)

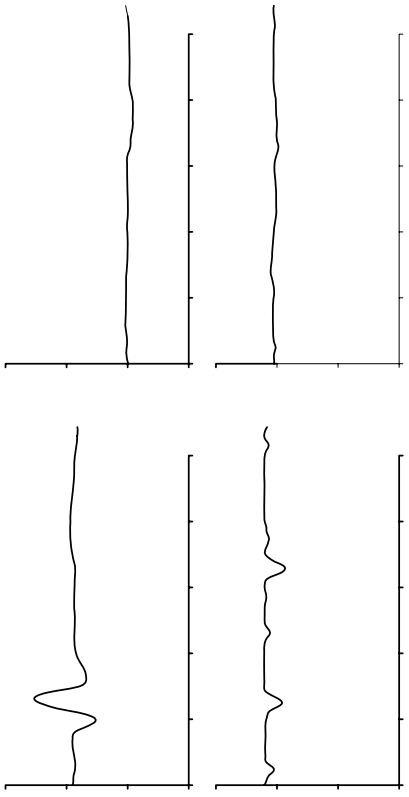

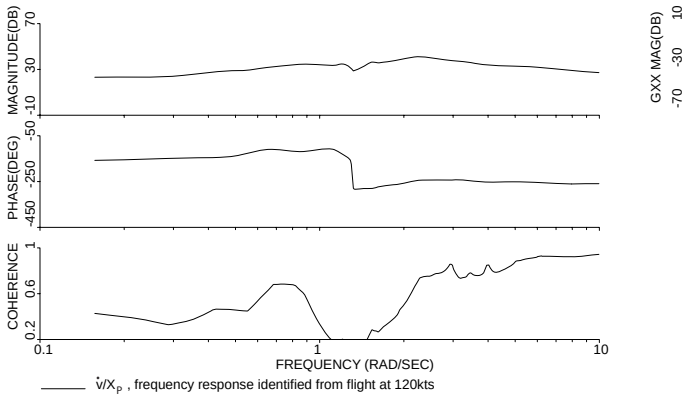

Figure 11. Pedal to lateral velocity response ($\dot{v}/\delta_{ped}$) at 120 knots.

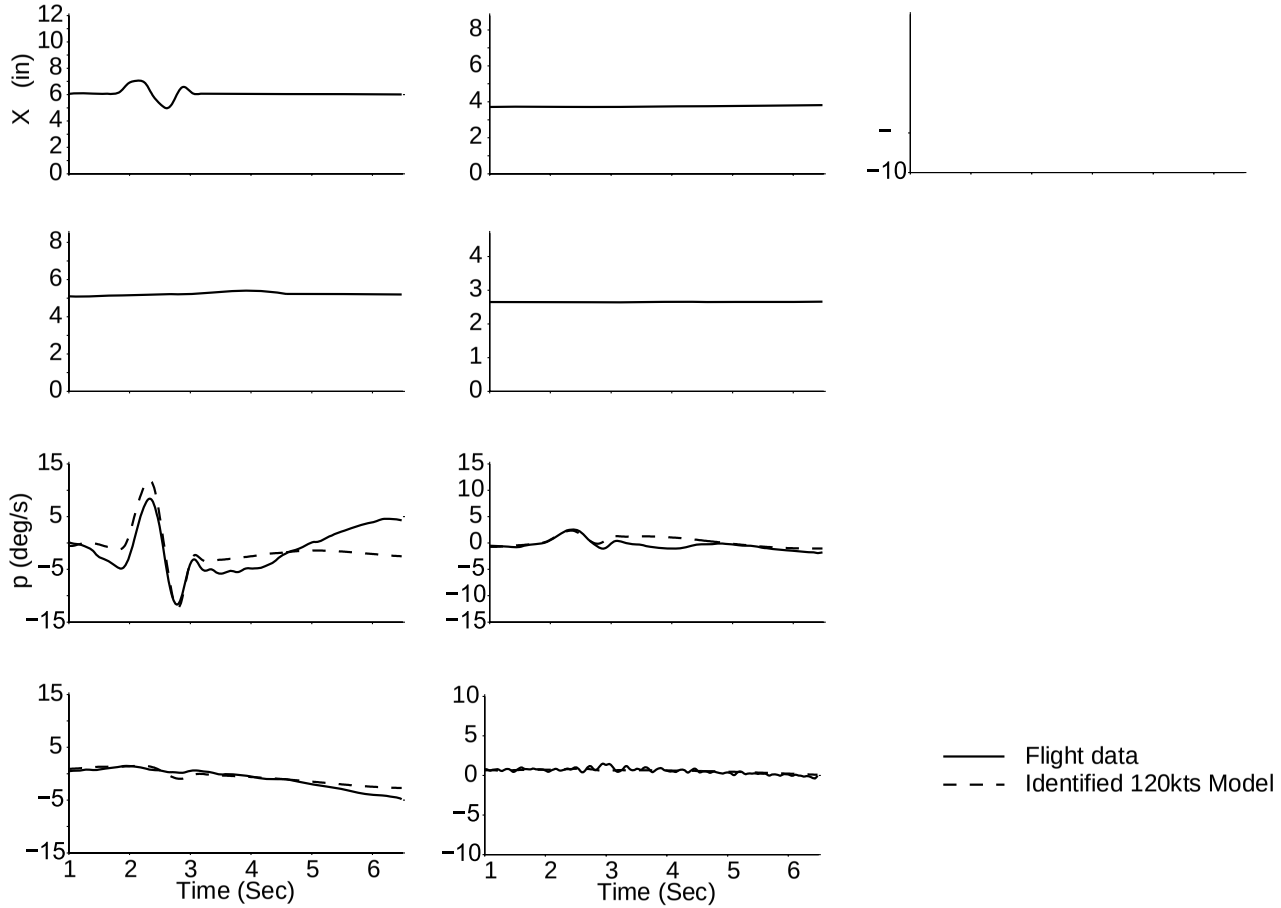
X (in)
p (deg/s)
Time (Sec)
Time (Sec)
Flight data
Identified 120kts Model

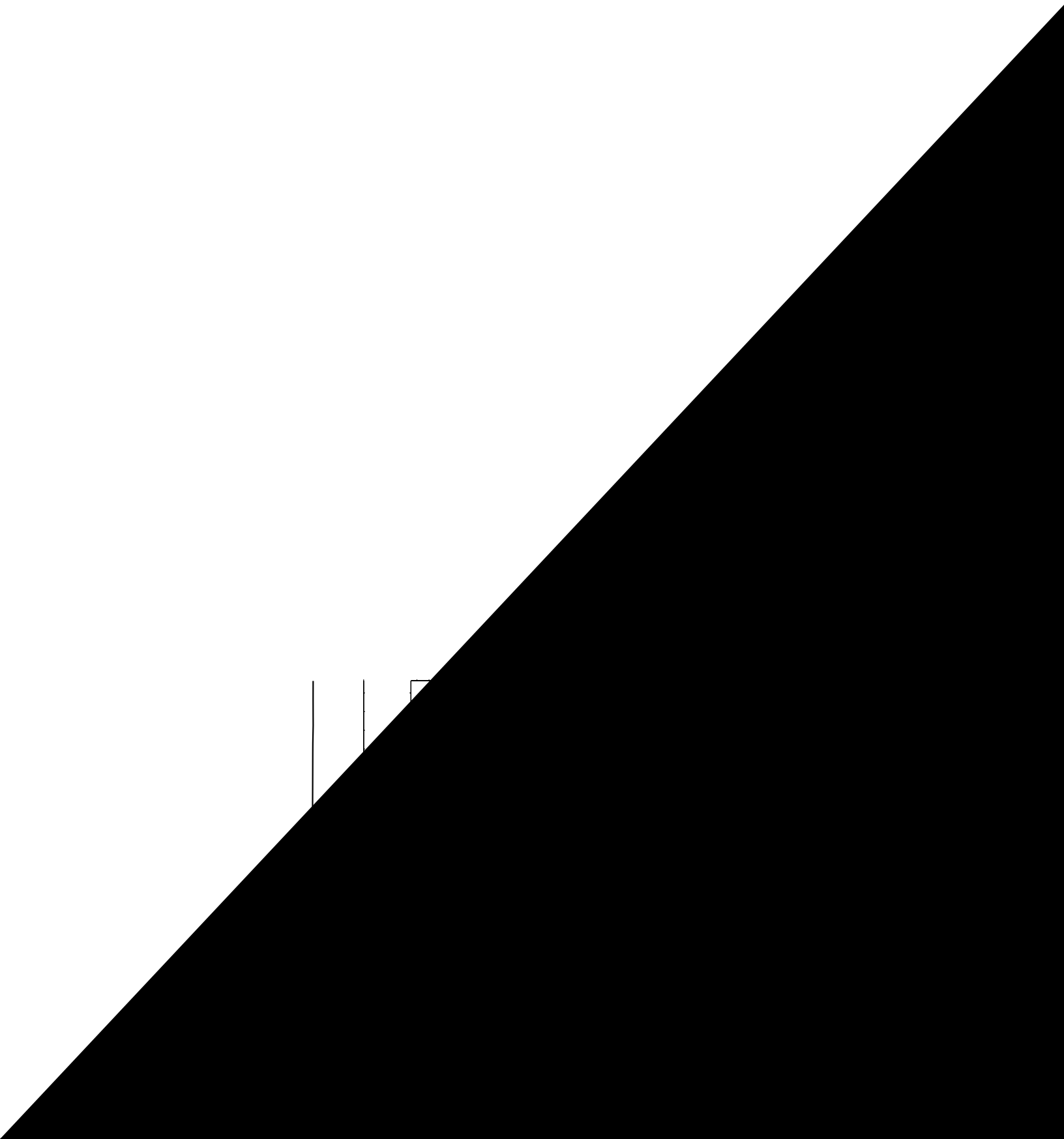

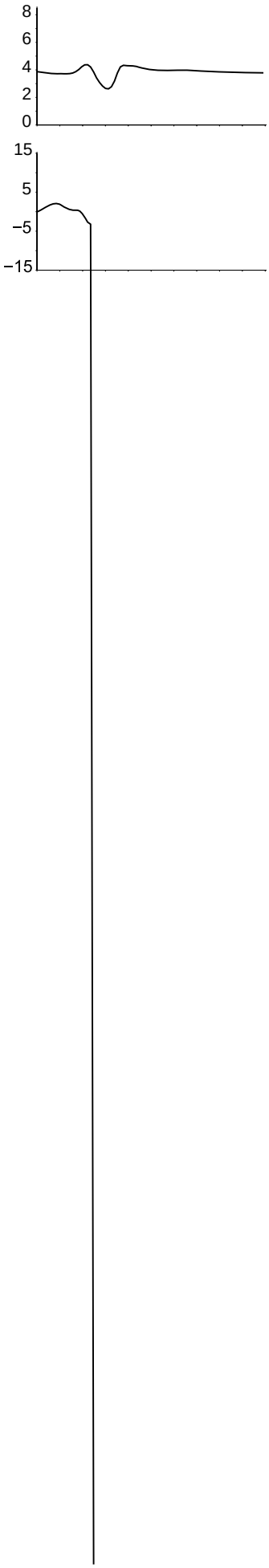
8
6
4
2
0
15
5
−5
−15

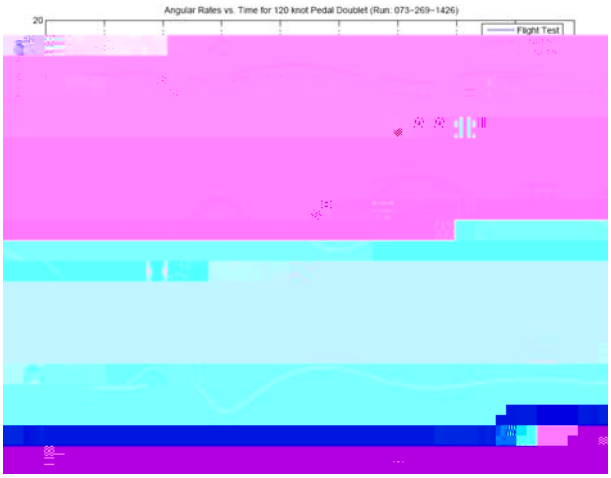

Figure 28. Pitch rate, roll rate and yaw rate vs. time for pedal doublet at 120 kts.

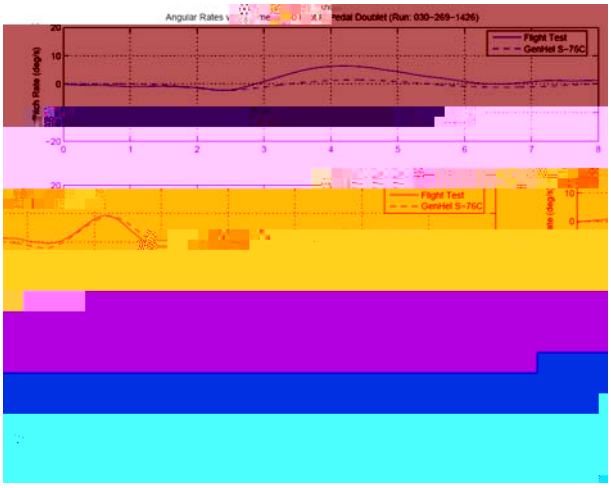

Figure 29. Pitch rate, roll rate and yaw rate vs. time for pedal doublet at 80 kts.

Table 2. Identified F-matrix parameters for hover model.

$-\omega_{ll_r}^2$	-651.9	1.241	0.4622
$-2\xi_{ll_r}\omega_{ll_r}$	-6.159	5.339	2.298
K_q			

Table 4. Cost functions for hover model.

Transfer Function	Cost
$\dot{u}/X_B$	47.383
p/X_B	84.46
q/X_B	83.157
a_x/X_B	124.340
a_z/X_B	149.784
$\dot{v}/X_A$	132.847
p/X_A	87.137
q/X_A	56.919
r/X_A	224.027
a_y/X_A	31.810
$(a_y)_2/X_A$	123.294
$\dot{v}/X_P$	26.947
p/X_P	71.222
r/X_P	129.88
a_z/X_P	155.966
$\dot{u}/X_C$	50.260
r/X_C	27.928
a_x/X_C	40.084
a_z/X_C	47.869
Average	89.227

Table 5. Identified F-matrix parameters for 120 knots model.

Derivative	Value	Cramer Rao (%)	Insensitivity (%)
X_u	-0.0457[a]	n/a	n/a
X_v	0[b]	n/a	n/a
X_w	0.0365	10.02	4.165
X_r	0[b]	n/a	n/a
$X_{\beta_{1c}}$	40.54	4.255	0.998
Y_u	0[b]	n/a	n/a
Y_v	-0.3441	5.716	0.805
Y_w	0[b]	n/a	n/a
Y_p	-7.047	5.969	1.512
Y_r	-3.417	38.88	8.083
$Y_{\beta_{1s}}$	-40.54[c]	n/a	n/a
Z_u	0.2561	15.47	2.531
Z_v	0[b]	n/a	n/a
Z_w	-0.3268	5.398	1.106
Z_p	0[b]	n/a	n/a
Z_q	-48.44	5.257	1.993

Z_r	0[b]	n/a	n/a
L_u	0[b]	n/a	n/a
L_v	-0.078[a]	n/a	n/a
L_w	0.0065	8.896	2.761
L_r	-2.173	15.53	2.867
$L_{\beta_{1s}}$	-62.55	3.143	0.5156
M_u	-0.0035	17.37	2.914
M_v	0[b]	n/a	n/a
M_w	0.0065	5.68	0.8366
M_r	0[b]	n/a	n/a
$M_{\beta_{1c}}$	-12.35	4.269	0.6264
N_u	0[b]	n/a	n/a
N_v	0.0041	15.69	3.551
N_w	0[b]	n/a	n/a
N_p	0.2233	9.558	2.3
N_q	-0.1611	8.373	2.03
N_r	-0.3[a]	n/a	n/a
$N_{\beta_{1s}}$	-9.252	4.871	0.8439
$N_{\beta_{1c}}$	1.589	8.274	2.309
τ_f	0.09916	2.803	0.7471
$Lf_{\beta_{1c}}$	-0.506	6.919	0.9594
$Mf_{\beta_{1s}}$	0.528	8.119	1.94
K_p	1.352[a]	n/a	n/a
ω_p^2	552.2[a]	n/a	n/a
$2\zeta_p\omega_p$	3.008[a]	n/a	n/a
$-\omega_{ll_r}^2$	-651.9[a]	n/a	n/a
$-2\xi_{ll_r}\omega_{ll_r}$	-6.128[a]	n/a	n/a
K_q	0.85[a]	n/a	n/a
ω_q^2	700.0[a]	n/a	n/a
$2\zeta_q\omega_q$	4.127[a]	n/a	n/a
$-\omega_{ll_{r2}}^2$	-651.9[c]	n/a	n/a
$-2\xi_{ll_{r2}}\omega 2_{ll_{r2}}$	-6.128[c]	n/a	n/a

a

Table 6. Identified G-matrix parameters for 120 knots model.

Derivative	Value	Cramer Rao (%)	Insensitivity (%)
X_{X_P}	0[b]	n/a	n/a
X_{X_C}	0.3843	10.07	4.04
Y_{X_p}	-5.023	22.14	3.161
Y_{X_C}	0[b]	n/a	n/a
Z_{X_B}	7.028	3.611	1.629
Z_{X_A}	0[b]	n/a	n/a
Z_{X_P}	0[b]	n/a	n/a
Z_{X_C}	-11.09	3.179	1.516
L_{X_P}	-0.4864	9.439	3.872
L_{X_C}	0[b]	n/a	n/a
M_{X_P}	0[b]	n/a	n/a
M_{X_C}	0.2648	3.308	1.195
N_{X_B}	0[b]	n/a	n/a
N_{X_P}	0.8534	2.701	0.9511
Lf_{X_B}	0.0359	4.882	0.6017
Lf_{X_A}	-0.0205	5.131	1.117
Mf_{X_B}	0.0461	4.083	0.6085
Mf_{X_A}	0.009	6.692	1.79
τ_{X_B}	0.0[b]	n/a	n/a
τ_{X_A}	0.0[b]	n/a	n/a
τ_{X_P}	0.0[b]	n/a	n/a
τ_{X_C}	0.1393	2.296	1.131

[a]Fixed in model structure.
[b]Eliminated during model structure determination.

Table 7. Cost functions for 120 knots model.

Transfer Function	Cost
$\dot{u}/X_B$	125.5
$\dot{v}/X_B$	76.13
$\dot{w}/X_B$	219.58
p/X_B	141.21
q/X_B	127.38
$q_{lead-lag}/X_B$	509.45
r/X_B	115
a_x/X_B	121.68
a_y/X_B	38.2
a_z/X_B	49.72
$(a_y)_2/X_B$	153.34
$(a_z)_2/X_B$	712.64
$\dot{v}/X_A$	76.13
$\dot{w}/X_A$	81.23
p/X_A	184.83
$p_{lead-lag}/X_A$	533.83
q/X_A	77.4
a_y/X_A	72.91
$(a_y)_2/X_A$	177.04
$\dot{v}/X_P$	99.28
$\dot{w}/X_P$	109.12
$/ \quad_P$	